Mugla Journal of Science and Technology

# INJECTABLE CMC–PVA HYDROGELS WITH DUAL HAEMOSTATIC AND ANTIOXIDANT ACTIVITY FOR SOFT TISSUE REPAIR

Banu KOCAAGA*, Faculty of Chemical and Metallurgical Engineering, Department of Chemical Engineering, Istanbul Technical University, Maslak, 34469 Istanbul, TURKIYE bkocaaga@itu.edu.tr
(https://orcid.org/ 0000-0001-6233-2463)
Atakan MERAN, Department of Bioengineering, Faculty of Engineering and Natural Sciences, Uskudar University, Istanbul, TURKİYE atakan.meran@uskudar.edu.tr
(https://orcid.org/ 0000-0001-8804-1365)

Received: 06.10.2025, Accepted: 28.10.2025 Research Article
*Corresponding author DOI: 10.22531/muglajsci.1797782

**Abstract**

*Injectable hydrogels that adapt to irregular and exudative wound geometries can shorten surgical procedures, enhance patient comfort, and reduce dressing frequency. Here, carboxymethyl-cellulose/poly(vinyl alcohol) (CMC–PVA) hydrogels loaded with procaine (PC) were developed as multifunctional wound dressings. Sequential gelation—ionic cross-linking of CMC with $Ca^{2+}$, electrostatic and hydrogen-bonding association of PC, and subsequent PVA incorporation—yields an interpenetrating network exhibiting shear-thinning viscosity and 74% self-healing recovery, ensuring facile syringe extrusion and rapid shape retention. Lap-shear tests revealed adhesive strengths of 0.8–1.1 MPa, while swelling ratios of 40–60 g $g^{-1}$ maintained tissue contact and hydration. Controlled release achieved 95% PC delivery within 6 h, enabling localized analgesia and 40% DPPH scavenging. Hemolysis was below 5 %, the blood-clotting index decreased from 92 % (control) to 28 %, and fibroblast migration remained unaffected after 48 h. SEM–EDS confirmed homogeneous morphology at moderate PC loading, whereas excessive drug induced microvoids. Experimental findings, supported by molecular dynamics simulations, indicated stiffness values compatible with dermal tissue mechanics. The developed PC-loaded CMC–PVA hydrogels combine injectability, bioadhesion, hemostasis, antioxidant activity, and cytocompatibility, offering a promising platform for soft-tissue regeneration and advanced wound management.*

**Keywords: Injectable hydrogel, Hemostatic activity, Controlled release, Na-CMC, Bioadhesion**

# YUMUŞAK DOKU YENILENMESI İÇİN BİYOAKTİF VE YAPIŞKAN ENJEKTE EDİLEBİLİR CMC–PVA TABANLI HİDROJELLER

**Özet**

*Düzensiz ve eksüdatif yara geometrilerine uyum sağlayabilen enjekte edilebilir hidrojeller, cerrahi sürenin kısalmasına, hasta konforunun artmasına ve pansuman değişimlerinin azalmasına katkı sağlar. Bu çalışmada, prokain (PC) yüklü karboksimetilselüloz/poli(vinil alkol) (CMC–PVA) hidrojeller çok işlevli yara örtüleri olarak geliştirilmiştir. Jelasyon; CMC'nin $Ca^{2+}$ ile iyonik çapraz bağlanması, PC'nin elektrostatik/hidrojen bağı etkileşimleriyle tutulması ve PVA'nın ağın güçlendirilmesiyle gerçekleştirilmiştir. Ortaya çıkan iç içe geçmiş ağ, kayma incelmesi ve %74 kendini iyileştirme göstererek kolay enjektabilite ve hızlı şekil korunumunu sağlamıştır. Lap-shear testinde 0.8–1.1 MPa yapışma kuvveti elde edilmiş; 40–60 g/g şişme oranları yakın doku teması ve sürekli hidratasyonu desteklemiştir. %95'e varan kontrollü PC salımı ve %40 DPPH giderimi sağlamıştır. Hemoliz <%5 düzeyinde kalmış, pıhtılaşma indeksi kontrolde %92 iken %28'e düşmüştür; çizik iyileşmesi testinde 48 saatte fibroblast göçü olumsuz etkilenmemiştir. SEM–EDS orta PC yüklemesinde homojen mikro yapı gösterirken, yüksek yükleme mikrogözenekler ve düşük modülle ilişkilendirilmiştir. Tüm atom düzeyi moleküler dinamikler dermal dokuya uygun mekanik sertlik aralığını doğrulamıştır. PC yüklü CMC–PVA hidrojeller; enjekte eidlebilir, güçlü doku yapışması, hemostatik etki, antioksidan kapasite ve hücre uyumluluğunu bir arada sunarak, geniş, anatomik olarak karmaşık veya cerrahi olarak eksize edilmiş doku defektleri için ileri düzey yara örtüleri olarak önemli bir potansiyel taşımaktadır.*

**Anahtar Kelimeler: Enjekte edilebilir hidrojel, Hemostatik aktivite, Kontrollü salım, Na-CMC, Biyoyapışkanlık**

**Cite**

**Kocaaga, B., Meran, A., (2025). "Injectable CMC–PVA Hydrogels with Dual Haemostatic and Antioxidant Activity for Soft Tissue Repair", Mugla Journal of Science and Technology, 11(2), 39-48.**

## 1. Introduction

Haemostasis, inflammation, proliferation, and remodelling constitute a tightly regulated cascade in wound healing [1]. Haemostasis rapidly prevents exsanguination and provides a provisional matrix via platelet aggregation and fibrin formation, followed by neutrophil–macrophage–mediated clearance and cytokine/ROS signalling in inflammation [2,3]. Effective repair requires a moist, oxygen-permeable milieu that modulates ROS and removes excess exudate to support re-epithelialisation, angiogenesis, and matrix remodelling.

Designing wound biomaterials therefore demands mechanical robustness, antimicrobial protection, and regenerative capacity, with tissue adhesiveness and intrinsic bioactivity being pivotal [4]. Hydrogels—hydrated, three-dimensional polymer networks—mimic the polysaccharide-rich ECM, establish a moist, permeable barrier against microbes, and support cell adhesion and migration [5–9]. Stiffness and resilience must approximate native cues to maintain coverage under physiological loads and guide tissue regeneration [10]. Recent advancements in polysaccharide-based hydrogels, such as alginate, hyaluronic acid, pectin, and chitosan systems, have exhibited improved biocompatibility, adjustable swelling, and biofunctional characteristics that facilitate regulated drug administration and expedited wound healing [11–14]. Among polysaccharides, CMC offers abundance, cytocompatibility, degradability, chemical stability, low immunogenicity, and mucoadhesion that enhances residence and drug retention [15–21], though neat CMC gels can lack strength and self-repair at dynamic sites [22].

To strengthen the network, PVA was integrated to form hydrogen-bonded, entangled, interpenetrating matrices with improved elasticity and toughness without sacrificing compatibility [23–26]. $Ca^{2+}$ bridging of carboxylates further reinforced the gel and supported rapid coagulation upon blood contact [27], consistent with the multifaceted roles of $Ca^{2+}$ in haemostasis, keratinocyte differentiation, fibroblast contraction, and angiogenesis [17,28]. An experimental–computational framework was adopted to link composition and supramolecular interactions to bulk properties, leveraging molecular simulations to inform formulation design. PC was selected as a multifunctional agent: beyond local anaesthesia via $Na^{+}$-channel blockade, it down-regulates NF-κB-dependent TNF-α/IL-6 signalling, mitigates oxidative stress, and promotes granulation and neovascularisation [29–33]. Controlled PC delivery from a haemocompatible hydrogel can synchronise analgesic, anti-inflammatory, and antioxidant actions with wound-healing timelines [6,34–36].

Herein we report an injectable CMC/PVA hydrogel ionically cross-linked by $Ca^{2+}$ and loaded with PC. The platform achieves rapid haemostatic sealing, intrinsic antioxidant activity with negligible haemolysis, and sustained PC release. Comprehensive characterisation (SEM–EDS, contact angle, oscillatory rheology, swelling, release kinetics, and hemocompatibility) establishes structure–property–function relationships, while all-atom molecular dynamics (LAMMPS) elucidates PC-mediated reinforcement at the molecular scale. The resulting material addresses mechanical, biochemical, and haemodynamic requirements for advanced wound care and provides a versatile basis for future tissue-regenerative applications.

## 2. Material and Methods

### 2.1. Molecular Dynamics Simulations

Detailed descriptions of the simulation setup and parameters are provided in the Supplementary Information section S.2.1.

### 2.2. Experimental Methods

#### 2.2.1. Materials

PVA, Mw ≈ 61 000 g $mol^{-1}$, Mowiol 10-98) and sodium hydroxide (NaOH) were obtained from Merck (Darmstadt, Germany). PC hydrochloride (PC) purchased from Sigma-Aldrich (Düsseldorf, Germany). NaCM was supplied by Ashland (Wilmington, USA). All chemicals were of analytical grade and used without further purification. Ultra-pure deionized (DI) water was employed in all experimental procedures.

#### 2.2.2. Preparation of CMC-PVA Hydrogel

CMC (30 % w/v) was dissolved in de-ionised water under continuous stirring (100 rpm) at 60 °C for 24 h until a clear solution formed. Calcium chloride ($CaCl_2$, 0.7 wt %; 70 mg per 10 g of solution) was then added at 37 °C to establish ionic cross-links and create a $Ca^{2+}$-stabilised CMC gel. An equivalent mass of PVA (30 % w/v), was subsequently incorporated, enabling hydrogen bonding and chain entanglement to reinforce the network. Finally, PC was introduced at 1.2, 2.4, or 4.8 mg $g^{-1}$ of wet hydrogel, generating the formulations designated CMC-PVA-P0, CMC-PVA-P1, CMC-PVA-P2, and CMC-PVA-P4, respectively (Table S1).

#### 2.2.3. Morphological and Thermal Analysis

Scanning electron microscopy (JSM-6390LV, JEOL, Tokyo, Japan) was employed to analyze the hydrogel microstructure. For sample preparation, specimens were snap-frozen in liquid nitrogen and fractured using precooled tweezers.

Differential scanning calorimetry (DSC) analysis was performed using a Perkin Elmer DSC 4000 (Perkin-Elmer Instruments, USA) under a nitrogen atmosphere (20 mL/min flow rate) [7].

#### 2.2.4. Swelling Behaviour

To assess the swelling behavior, lyophilized hydrogel discs (diameter: 10 mm) were initially weighed ($W_D$) and immersed in 25 mL of Tris buffer (pH 6.4) at 37 °C. At

predetermined time intervals, samples were removed, gently blotted to eliminate residual surface moisture, and reweighed in the swollen state ($W_S$) [7]. The swelling ratio (SR) was calculated according to the following equation:

$$\text{Swelling (\%)} = \frac{W_S - W_D}{W_D} \times 100 \quad \text{Equation 1}$$

### 2.2.5. *In vitro* Drug Release

In-vitro PC release was monitored by UV–visible spectroscopy. Fresh hydrogel discs were placed in 50 mL Tris buffer (pH 7.4) and incubated at 37 °C with orbital shaking (100 rpm) in sealed vials. At scheduled intervals, 1 mL of the medium was withdrawn, replaced with fresh buffer, and analyzed at 290 nm using a UV/Vis spectrophotometer (PerkinElmer, Waltham, MA, USA) (12, 37). PC concentration was calculated with the Beer–Lambert law from a calibration curve ($R^2 > 0.999$) generated from standard solutions [38].

### 2.2.6. Rheological Analysis

Rheological properties were analysed using an Anton Paar MCR 301 rheometer (PP25 geometry, 1 mm gap) with a Peltier-controlled system and solvent trap [6–8]. Strain-sweep tests (25 °C; 0.1–1000 % strain; 6.28 rad $s^{-1}$) defined the linear viscoelastic (LVE) region, determining the critical strain (γL), storage modulus (G'LVE), and flow point at the G/G″ crossover (γf, Gf), which indicated the onset of structural breakdown. Frequency sweeps (0.1–100 rad $s^{-1}$) within the LVE region quantified frequency-dependent G, G″, and tanδ, revealing network rigidity and viscoelastic damping characteristics.

Thixotropic recovery was evaluated at 25 °C and 6.28 rad $s^{-1}$ using a multi-cycle strain protocol alternating low (1 %) and high (1000 %) deformations. Recovery of G′ during the low-strain intervals reflected the self-healing and structural reversibility of the hydrogels—key for injectability and shape-conformability. The recovery rate after the sixth cycle was determined as

$$\text{RS (\%)} = 100 - \left[\frac{G'_{11}}{G'_1} \text{x } 100\right] \quad \text{Equation 2}$$

where $G'_1$ and $G'_{11}$ are the average storage moduli measured in the first and eleventh steps, respectively.

### 2.2.7. Adhesion Strength

Lap-shear adhesion strength was determined according to ASTM F2255-05 [30] using an Instron 5943 (1 kN) and, for higher loads, a Devotrans DVT-UZMK (20 kN). Stainless-steel plates (10 × 2.5 × 1 cm) were cleaned with ethanol, air-dried, and assembled in a standard single-lap configuration. Hydrogel specimens (2.5 × 1 cm) were applied to the overlap region to ensure uniform contact during testing [35]. Samples were pulled at 1 mm $min^{-1}$ until failure. Lap-shear strength (τ) was calculated using

$$\tau = \frac{F_{max}}{S} \quad \text{Equation 7}$$

where τ is the lap-shear stress (Pa), Fmax the maximum load (N), and S the overlap area ($m^2$) [6].

### 2.2.8. Hemolysis Activity

Hemocompatibility was assessed using bovine erythrocytes. Whole blood, anticoagulated with 3.2% (w/v) sodium citrate, was centrifuged to isolate RBCs, which were subsequently washed with PBS (pH 7.4) and re-suspended to a final concentration of 10% (v/v) in PBS. Hydrogel discs (Ø 4 mm) were incubated with 1 mL of the RBC suspension at 37 °C for 2 h. PBS:RBC (1:1, v/v) and distilled water:RBC (1:9, v/v) served as negative and positive controls, respectively. Following incubation and centrifugation, 100 µL of each supernatant was transferred to a 96-well plate, and absorbance was measured at 540 nm using a microplate reader (SPECTRAmax 340PC). Hemolysis (%) was determined based on absorbance values.

$$\text{Hemolysis (\%)} = \frac{OD_{sample} - OD_{negative\ control}}{OD_{positive\ control} - OD_{negative\ control}} \times 100 \quad \text{Equation 3}$$

### 2.2.9. *In vitro* Wound Healing Assay

PCS-201-012 human dermal fibroblasts (ATCC, Manassas, VA, USA) were seeded into collagen-coated 24-well plates and cultured at 37 °C in a humidified atmosphere containing 5 % $CO_2$. After the cells reached confluence, a linear scratch was introduced into each monolayer with a sterile pipette tip. Wells were then supplemented with either culture medium alone (control) or medium containing the test hydrogels, and incubation continued for 48 h without medium replacement. Phase-contrast micrographs of the wound area were acquired at 0, 24, and 48 h using an inverted microscope (Carl Zeiss, Jena, Germany). Each condition was tested in duplicate.

### 2.2.10. *In vitro* Blood Clothing Assay

Whole bovine blood was obtained in sodium-citrate tubes from a local abattoir. Circular hydrogel discs (Ø 4 mm) were pre-swelled in PBS for 15 min and transferred to 1.5 mL microtubes. Then, 50 µL of citrated whole blood was added to each sample, followed by 4 µL of 0.2 M $CaCl_2$ to initiate coagulation. After incubation at 37 °C for defined durations, 1 mL of distilled water was added to lyse uncoagulated erythrocytes. Supernatants were collected, and absorbance was measured at 540 nm using a microplate reader (SPECTRAmax 340PC). The blood-clotting index (BCI) was calculated using Equation 4:

$$\text{BCI (\%)} = \frac{A}{B} x100\% \quad \text{Equation 4}$$

where A is the absorbance of the test sample and B is the absorbance of the reference (blood without hydrogel).

### 2.2.11. Antioxidant Assay

The radical-scavenging ability of the hydrogels was quantified by a modified 2,2-diphenyl-1-picrylhydrazyl (DPPH•) assay [39]. Disc-shaped specimens (3 mm diameter) were extracted in 1 mL methanol at 37 °C for 1 h in the dark. Each extract (1 mL) was combined with an equal volume of 200 µM DPPH solution in methanol and incubated at room temperature for 30 min under light-protected conditions. Absorbance at 517 nm was measured using a microplate reader (SPECTROstar® Nano, BMG LABTECH, Ortenberg, Germany). The percentage of DPPH scavenging was calculated with

Equation 5:

$$\text{DPPH Scavenging Activity (\%)} = \frac{\text{OD}_{\text{control}} - \text{OD}_{\text{sample}}}{\text{OD}_{\text{control}}} \times 100 \quad \text{Equation 5}$$

where OD_control denotes the absorbance of DPPH solution alone and OD_sample is the absorbance of the extract–DPPH mixture.

## 3. Result and Discussion

Effective wound healing and tissue regeneration require biomaterials that support cellular viability, promote hemostasis, exhibit antioxidant activity, and facilitate re-epithelialization. Hydrogels intended for such applications must not only provide a cytocompatible environment but also maintain mechanical stability under physiological conditions to preserve these biological functions. In this context, the present study explores the therapeutic potential of CMC–PVA–PC hydrogels, focusing on their ability to integrate biological performance with mechanical integrity. The incorporation of PC, known for its anti-inflammatory and membrane-stabilizing effects, was hypothesized to enhance both bio-functionality and dynamic adaptability. To evaluate their translational relevance, the hydrogels were subjected to detailed rheological characterization and all-atom molecular dynamics simulations, assessing how increasing PC content influences matrix stiffness, viscoelastic recovery, and network resilience. This dual analysis offers insights into the scaffold's capacity to sustain tissue-level mechanical loads, self-heal after stress, and conform intimately to irregular wound geometries—key features for promoting angiogenesis, minimizing infection risk, and accelerating functional tissue restoration

### 3.1. Molecular Dynamic Simulations

#### 3.1.1 Mechanical Property Analysis

Figure 1 illustrates the mechanical performance of CMC/PVA/procaine blends as a function of procaine concentration. Young's modulus (Figure 1a) showed a strong linear correlation ($R^2$ = 0.967), increasing from 0.036 to 0.048 GPa—a 33% enhancement—indicating that procaine molecules reinforce the matrix through additional intermolecular interactions with CMC and PVA chains. Similarly, the ultimate tensile strength (Figure 1b) increased linearly from 290 MPa to 395 MPa ($R^2$ = 0.980), confirming the strengthening effect of procaine. Yield stress (Figure 1d) exhibited the strongest correlation ($R^2$ = 0.999), reflecting a highly predictable strengthening behavior beneficial for material design. Toughness (Figure 1c) increased significantly from 14.8 to 22.5 MJ/m$^3$, representing a 52% improvement in the material's energy absorption capacity. This substantial gain indicates that procaine enhances not only stiffness and strength but also the ability of the polymer matrix to dissipate mechanical energy under load. The improvement is likely due to additional hydrogen bonding and secondary interactions that enable more uniform stress distribution during deformation. In contrast, yield strain (Figure 1e) remained nearly constant at 8–9% ($R^2$ = 0.111), showing that procaine mainly influences strength-related properties rather than the onset of plastic deformation.

### 3.2. Experimental Methods

In the present work, we developed a supramolecular highly transparent injectable hydrogel composed of CMC and PVA, crosslinked by $Ca^{2+}$ ions and loaded with PC, to address three major shortcomings of conventional hydrogels: mechanical fragility, limited bioactivity, and poor stability under repeated mechanical stress. $Ca^{2+}$ ions first coordinate with the carboxylate groups of CMC, generating an ionically cross-linked backbone that regulates pore architecture and water uptake [43]. Interpenetrating PVA chains reinforce this backbone through extensive hydrogen bonding with both $Ca^{2+}$-stabilised carboxylates and residual CMC hydroxyls, imparting cohesive strength and viscoelastic stability [44-45]. Protonated PC molecules electrostatically associate with unoccupied carboxylate sites and are further retained within hydrophilic PVA microdomains, producing a uniform drug distribution [6,12,46]. The overall mechanism of hydrogel assembly is illustrated in Scheme 1.

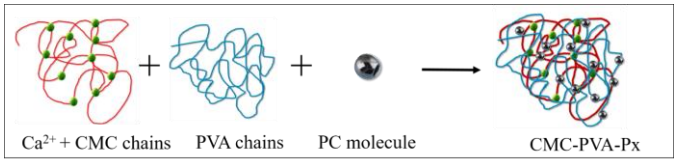


Scheme 1. Schematic representation of hydrogel formation: Ionic crosslinking between $Ca^{2+}$ ions and CMC chains establishes the initial gel network, followed by physical entanglement and hydrogen bonding with PVA chains. The incorporation of PC molecules introduces additional supramolecular interactions, resulting in a reinforced CMC–PVA–Px hydrogel matrix.

#### 3.2.1. Morphological and Thermal Analysis

DSC revealed progressive thermal stability with increasing PC loading (ΔT ≈ +25 °C; details in Supplementary Figure S1.

Detailed SEM–EDS images and spectra for all formulations are included in the Supplementary Information (Figure S2).

### 3.2.2. Rheological Performance of the Hydrogels

The viscoelastic behaviour of the PVA/CMC hydrogels affected injectability, mechanical strength, and dimensional stability [7,8,47]. The hydrogels were assessed by four rheological analyses to verify their suitability as injectable wound dressings: (i) Amplitude sweep defined the linear viscoelastic region (LVE) and flow point, indicating tolerance to the high shear applied during syringe extrusion. (ii) Frequency sweep measured storage (G′) and loss (G″) moduli over 0.1–100 rad $s^{-1}$, covering deformation rates relevant to normal tissue movement.

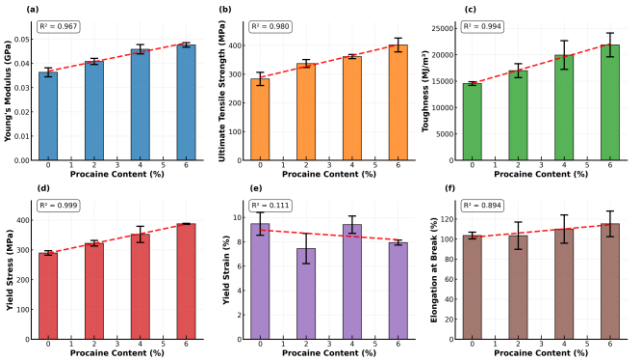


Figure 1. Mechanical properties of CMC/PVA/procaine polymer blends as a function of procaine content: (a) Young's modulus, (b) ultimate tensile strength, (c) toughness, (d) yield stress, (e) yield strain, and (f) elongation at break. Error bars represent standard deviation, and dashed lines show linear trend fits with corresponding $R^2$ values.

Damping factor (tan δ) calculations compared viscous and elastic contributions across the tested range, providing a concise measure of energy dissipation (iii) The thixotropic oscillation strain test was performed with a frequency of 6 Hz to demonstrate the capacity of the sample for arising from reversible $Ca^{2+}$ coordination, hydrogen bonding, and chain entanglement syringe delivery and rapid self - healing [6,48,49].

Amplitude-sweep testing revealed PC-dependence in the viscoelastic response of $Ca^{2+}$-bridged CMC–PVA hydrogels. Throughout the linear strain window, G′ exceeded G″ for every formulation, confirming elastic preference; both moduli diminished once the critical strain was surpassed, indicating partial disruption of ionic junctions [50].

The CMC-PVA-P4 exhibited the smallest G′ and the earliest G/G″ crossover, findings that align with weaker chain interactions and the micro-voids observed by SEM (Figure S2 a-c). In contrast, intermediate PC levels expanded the LVE and sustained elastic superiority, whereas excessive loading reduced structural stiffness.

Frequency-sweep measurements (0.1–100 rad $s^{-1}$, Figure 2b) confirmed to power-law relationships (G′ ∝ ω^0.77; G″ ∝ ω^0.73), a characteristic feature of an entanglement-controlled supramolecular network in which segmental motion becomes progressively restricted at higher oscillation rates [24-28]. Across the measured frequency G′ remained above G'', reflecting a dual cross-link structure that combines fast, reversible $Ca^{2+}$ bridges with slower physical associations among PVA segments [29].

The damping factor (tan δ = G″/G′) decreases from 2.2 in CMC-PVA-P0 to 1.0, 0.85, and 0.70 in CMC-PVA-P1, CMC-PVA-P2, and CMC-PVA-P4, respectively (Table S1, Figure 5d), signifying a progressive shift toward elastic dominance as PC content increases as indicated moleculer dynamic simulation studies (Figure 1, Figure 2). In the CMC–PVA–P0 hydrogel, high damping indicates marked energy dissipation; the matrix is governed principally by $Ca^{2+}$ bridges between CMC carboxylates, which allow considerable chain mobility, resulting in a viscoelastic response dominated by the viscous component. Introducing PVA provides extensive hydroxyl functionality, while PC contributes secondary amine and ester groups; both species establish additional hydrogen bonds with CMC carboxylates and PVA hydroxyls, forming a denser array of transient cross-links. These supplementary interactions hinder polymer chain mobility, suppress viscous dissipation, and consequently reduce tan δ. The significant reduction observed for CMC–PVA–P1 and CMC–PVA–P2 indicates that moderate drug incorporation effectively balances cohesive strength and molecular mobility—properties required for conformability and self-healing.

Although CMC–PVA–P4 exhibits the lowest tan δ, its previously observed decrease in G′ suggests that excessive PC disrupts the $Ca^{2+}$ coordination network, reducing absolute stiffness while still limiting energy dissipation through abundant hydrogen bonding. Overall, the tan δ profile confirms a synergistic interplay between $Ca^{2+}$ bridges, polymer entanglement, and PC-mediated hydrogen bonding, with intermediate drug loading providing the most favourable viscoelastic signature for dynamic wound environments. Frequency sweep analysis (Figure 2e) confirmed pseudoplastic behaviour for all CMC–PVA hydrogels, with complex viscosity following η* = K ω^−n (n = 0.60–0.84, $R^2$ > 0.92). CMC–PVA–P0 exhibited the most marked rate dependence (n ≈ 0.84) and the lowest zero-frequency modulus, consistent with a network stabilized mainly by $Ca^{2+}$ coordination. Incorporation of PC at higher concentrations (CMC–PVA–P2 and CMC–PVA–P4) led to a reduction in the initial plateau modulus and yielded intermediate slope values (n≈0.69) in the frequency-dependent complex viscosity profile. These results suggest that elevated PC levels partially displace $Ca^{2+}$-mediated ionic bridges and increase the polymer chains' segmental mobility. Despite this softening effect, the formulation retained characteristic shear-thinning behavior, ensuring facile injectability under high shear and adequate mechanical integrity upon cessation of stress. The rheological signature, in combination with reduced damping factor (tan δ), reflects the formation of a more dynamic yet cohesive supramolecular network,

suitable for in situ delivery and conformal contact with irregular wound topographies.

Six-cycle strain sweep analysis showed rapid modulus restoration, confirming reversible network reformation (Figure 2h-k). Relative recovery decreased from 73.6 % (CMC–PVA–P0) to 66.8 %, 54.3 %, and 34.3 % for CMC–PVA–P1, CMC–PVA–P2, and CMC–PVA–P4, consistent with the progressive decrease in damping factor 0.93→0.90→0.78→0.56 (Table S1). Moderate drug loading thus maintains sufficient chain mobility for bond re-formation, whereas excessive levels restrict diffusion and compromise self-repair.

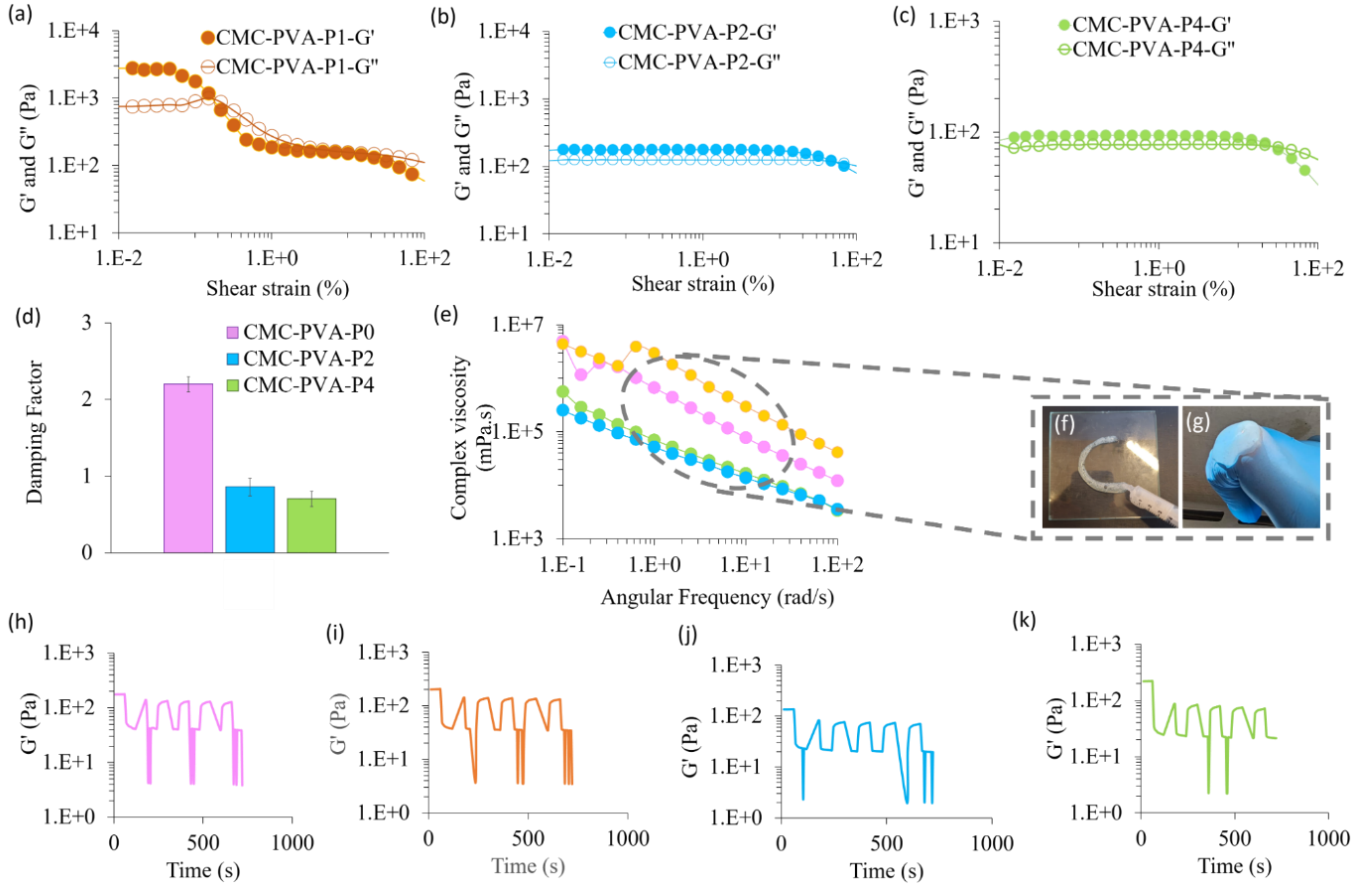


Figure 2. Rheological characterization of CMC–PVA hydrogels. Strain sweep curves of (a) CMC–PVA–P1, (b) CMC–PVA–P2, and (c) CMC–PVA–P4 showing storage modulus (G′ ) and loss modulus (G″ ) over the shear strain range. (d) Damping factor (tan δ) values indicate a shift toward elastic behavior with increasing PC concentration. (e) Complex viscosity. Insets (f–g) demonstrate injectability and shape retention. (h–k) Thixotropic time sweep profiles showing G′ recovery under cyclic high–low strain (1000%–1%), indicating the thixotropic/self-healing behavior of (h) CMC–PVA–P0, (i) CMC–PVA–P1, (j) CMC–PVA–P2, and (k) CMC–PVA–P4 formulations.

### 3.2.3. Adhesive Strength

Lap-shear study demonstrated a consistent enhancement in adhesive strength along with increasing PC content (Table S1, Figure 3a). underlying adhesion results from $Ca^{2+}$ bridging between CMC carboxylates and collagen nucleophiles, enhanced by hydrogen bonding among PVA hydroxyls, interfacial water, and neighboring CMC chains. The increasing addition of PC enhances interfacial bonding by facilitating electrostatic interactions between protonated amines and anionic ECM domains, promoting further hydrogen bond formation through amide and carbonyl groups, and improving wettability due to aromatic moieties that increase the actual contact area. Figure 3b–d illustrates that the hydrogels preserve adhesion under inversion and shear, hence validating stable, tissue-like interfaces [6]. Improved adhesion provides prolonged hydrogel-wound contact, inhibits exudate accumulation, preserves hydration, and minimizes re-bleeding or detachment during movement.

### 3.2.4. Swelling Analysis

The swelling characteristics of the hydrogels were assessed under pH 7.4 conditions using a tris buffer. The results demonstrated that the drug-free hydrogel (CMC-PVA-P0) absorbs water progressively, reaching a maximum swelling ratio of 29.2±3.4 g $g^{-1}$ at 200 min before gradual relaxation reduces its mass (Figure 4a). Adding 1.2 mg $g^{-1}$ PC (CMC-PVA-P1) increases the peak to 37.9±1.5 g $g^{-1}$ and delays it to ≈300 min, consistent with additional hydrogen-bond sites that elevate osmotic uptake while maintaining network integrity. Higher PC levels (CMC-PVA-P2, CMC-PVA-P4) display significantly faster water uptake, reaching 57.3±6.8 g $g^{-1}$ (90 min) and 48.4±4.5 g $g^{-1}$ (55 min), respectively, followed by a sharp decline demonstrating degradation of the hydrogels .The rapid water uptake can be attributed to two interrelated mechanisms: (i) the p-aminobenzoate segment of PC introduces extra hydrophilic and ionic groups that increase the chemical potential of water within the matrix, and (ii) protonated amines partially displace $Ca^{2+}$ from CMC carboxylates, lowering the effective cross-link density and creating larger aqueous channels. Once a critical hydration level is reached, reduced coordination allows chain re-association, leading to network contraction and water expulsion.

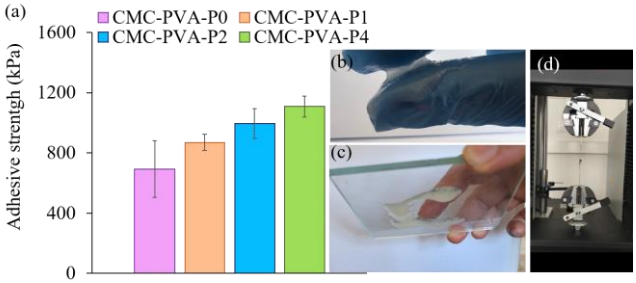


Figure 3. (a) Lap-shear analysis results showing the adhesive strength of CMC-PVA hydrogels with increasing PC content, indicating a PC concentration-dependent improvement in adhesion performance. (b) Visual demonstration of hydrogel adherence to a gloved fingertip, highlighting its strong tissue-like adhesion. (c) Hydrogel lettering remains attached to an inverted glass substrate without detachment or flow, confirming interfacial stability under gravity. (d) Representative image of the lap-shear analysis setup used for quantitative adhesive strength measurements.

### 3.2.5. Drug Release Behaviour

The release profiles aligned with the swelling data. CMC-PVA-P2 and CMC-PVA-P4, which exhibit the most rapid initial swelling, approach complete PC release (≈100 %) within 120–150 min, reflecting high diffusional flux through the transiently expanded pore network (Figure 4b). In contrast, CMC-PVA-P1 displays a biphasic pattern: an early burst to ≈40 % during the first hour, governed by surface diffusion, followed by a slower stage that reaches ≈95 % only after ≈400 min. The moderate and prolonged swelling of CMC-PVA-P1 restricts convective transport, enabling sustained diffusion through a comparatively denser matrix.

These findings confirm that PC content governs water uptake, cross-link stability, and release kinetics in an interdependent manner. Moderate loading (CMC-PVA-P1) affords extended hydration and prolonged drug delivery—attributes advantageous for continuous analgesia and exudate control—whereas higher loadings (CMC-PVA-P2, CMC-PVA-P4) provide rapid release appropriate for immediate pain relief but show reduced structural persistence under prolonged exposure.

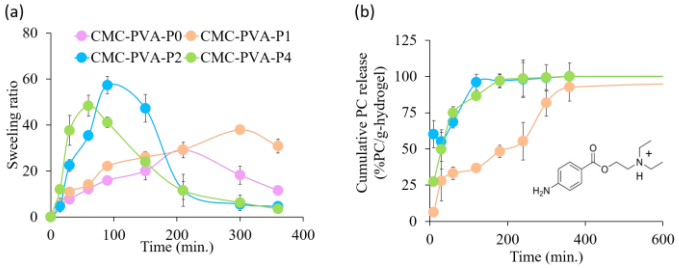


Figure 4(a) Swelling behavior of CMC-PVA hydrogels with varying PC content over time, (b) Cumulative PC release profiles from the hydrogels. The inset illustrates the chemical structure of protonated PC, the active agent incorporated within the hydrogel network.

### 3.2.6. Hemolysis Analysis

Hemolysis testing, conducted in accordance with ISO 10993-4, showed that the PVA/CMC–$Ca^{2+}$ hydrogel induced negligible erythrocyte lysis (< 2 %), comparable to the PBS (negative) control and well below the 5 % cytocompatibility limit (Figure 5a). Visual inspection proved the spectrophotometric data: supernatants from hydrogel incubations remained essentially clear. The low hemolytic index is attributed to the near-neutral pH of the hydrogel and the protective hydration layer provided by surface hydroxyl and carboxylate groups, which minimise electrostatic interactions with red-cell membranes and prevent osmotic imbalance. These findings confirm that the supramolecular PVA/CMC network is hemocompatible and suitable for direct contact with blood [51].

### 3.2.7. *In vitro* Wound Healing Analysis

A scratch (wound-healing) assay was used to assess the influence of the CMC-PVA-P4 on fibroblast migration (Figure 5b). After 48 h, the extent of gap closure was statistically indistinguishable from that of the untreated control ($p > 0.05$), indicating that the hydrogel do not impair fibroblast migration capacity [8].

### 3.2.7. Blood Clothing Analysis

Immediate blood coagulation is crucial in trauma and post-operative management, since extended bleeding impairs perfusion and hinders healing. Porous, hydrophilic hydrogels accelerate coagulation by absorbing plasma, concentrating blood components and establishing a $Ca^{2+}$-rich environment that facilitates fibrinogenesis [52]. The clotting index diminished from around 95% (control) to around 45% for

CMC-PVA-P0 and approximately 28% for CMC-PVA-P4, signifying enhanced coagulation (Figure 5c). The drug-free gel increases factor concentration through fast water absorption[43], whereas PC strengthens blood coagulation through electrostatic interactions with fibrinogen and erythrocyte membranes, facilitating platelet adhesion and aggregation [52]. The synergistic reactions provide a more compact fibrin network and expedited clotting, incorporating haemostatic, antioxidant, and analgesic properties advantageous for exudative and surgical wounds.

### 3.2.9. Antioxidant Analysis

Reactive oxygen species (ROS) surge during the inflammatory phase of cutaneous repair, where they serve as bactericidal agents but, when overproduced, trigger collateral damage to extracellular matrix (ECM) proteins, impede fibroblast migration, and prolong inflammation. DPPH-scavenging assays demonstrated negligible antioxidant capacity for the drug-free hydrogel (CMC-PVA-P0), whereas the PC-loaded variant (CMC-PVA-P3) removed approximately 40% of DPPH radicals—half the activity of the ascorbic-acid standard (90 %) (Figure 5d). This activity is attributed to facile electron transfer from the para-aminobenzoate segment of PC and its tertiary amine, which stabilise the DPPH radical via proton-coupled electron donation [53]. Within the $Ca^{2+}$-bridged CMC-PVA network, PC molecules are retained through hydrogen bonding with carboxylate groups of CMC and hydroxyl groups of PVA, facilitating sustained release while maintaining local concentrations sufficient for ROS quenching. By moderating oxidative stress, the PC-enriched hydrogel is expected to minimise matrix degradation, limit cytokine overexpression, and promote orderly transition to the proliferative phase, thereby accelerating granulation tissue formation and overall wound closure.

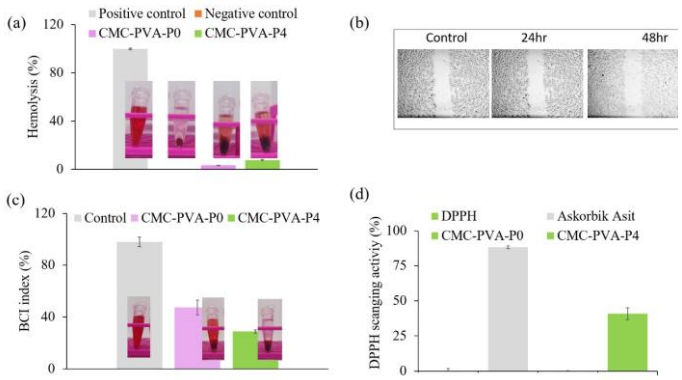


Figure 5. (a) Hemolysis percentages of hydrogel formulations compared to positive and negative controls. (b) In vitro wound-healing assay of CMC–PVA–P4 over 48 h. (c) Whole-blood clotting index (BCI) analysis. (d) DPPH radical scavenging activity, with ascorbic acid shown as a positive control for comparison.

## 4. CONCLUSION

Injectable hydrogels have been developed to meet critical clinical demands, including the management of post-surgical bleeding and accurate sealing of irregular tissue defects, where traditional dressings frequently lack consistent adhesion and efficacy. In this context, PC-loaded CMC–PVA hydrogels demonstrate physicochemical and biological properties appropriate for advanced wound-dressing applications. DSC evaluations indicated improved thermal stability with PC integration, while rheological assessments exhibited significant elasticity and shear-thinning characteristics, facilitating easy injection and rapid recovery. The CMC–PVA network demonstrated self-healing via $Ca^{2+}$ coordination and polymer entanglement, offering durable structure and consistent tissue adhesion that surpasses fibrin glues. Analyses of swelling and release validated extended hydration and continuous PC delivery, facilitating exudate management and localized pain relief. The materials demonstrated significant antioxidant and hemostatic properties while ensuring superior fibroblast compatibility. Molecular dynamics simulations confirmed these results by associating increased hydrogen-bonding density with a higher elastic response within the dermal modulus range. Individually, CMC contributed to hydrophilicity and water absorption capacity, regulating swelling and diffusion behavior, while PVA enhanced mechanical integrity, elasticity, and cytocompatibility through hydrogen bonding and chain entanglement. These data collectively demonstrate that CMC–PVA-P2 is a durable and versatile injectable hydrogel, exhibiting mechanical strength, biological efficacy, and cytocompatibility for advanced wound treatment. Future investigations are envisaged to evaluate the in vivo performance and long-term biocompatibility of the CMC–PVA hydrogel system.

## 5. Acknowledgment

This work is supported by İTU BAP under the project titled “Injectable, Self-Healing VEINOGRAP Hydrogel That Actively Supports Vascular Regeneration”, Project No: MAB-2024-45518. The author thanks Assoc. Prof. Ayça Bal Öztürk and Gülşah Torkay for their valuable assistance in cell experiments.

## 6. References

[1] Bennison LR, Miller CN, Summers RJ, Minnis AMB, Sussman G, McGuiness W., “The pH of wounds during healing and infection: a descriptive literature review”, Wound Pract Res J Aust Wound Manag Assoc, 25(2), 63–9, 2017.

[2] Li A., Ma B., Hua S., Ping R., Ding L., Tian B., et al., “Chitosan-based injectable hydrogel with multifunction for wound healing: A critical review”, Carbohydr Polym, 333(December 2023), 2024.

[3] Wang PH., Huang BS., Horng HC., Yeh CC., Chen YJ., “Wound healing”, J Chinese Med Assoc, 81(2), 94–101, 2018.

[4] Ma Z., Bao G., Li J., “Multifaceted Design and Emerging Applications of Tissue Adhesives”, Adv Mater, 33(24), 1–29, 2021.

[5] Güner OZ., Cam C., Arabacioglu-Kocaaga B., Batirel S., Güner FS., “Theophylline-loaded pectin-based hydrogels. I. Effect of medium pH and preparation

conditions on drug release profile", J Appl Polym Sci, 135(38), 2018.
[6] Zhao Y., Song S., Ren X., Zhang J., Lin Q., Zhao Y., "Supramolecular adhesive hydrogels for tissue engineering applications", Chem. Rev., 122(6), 5604–5640, 2022.
[7] Kocaaga AB., Kurkcuoglu O., Tatlier M., Batirel S., Guner FS., "Low-methoxyl pectin–zeolite hydrogels controlling drug release promote in vitro wound healing", J Appl Polym Sci, 136(24), 1–16, 2019.
[8] Kocaaga B., Kurkcuoglu O., Tatlier M., Dinler-Doganay G., Batirel S., Güner FS., "Pectin–Zeolite-Based Wound Dressings with Controlled Albumin Release", Polymers (Basel), 14(3), 2022.
[9] Grieco M., Ursini O., Palamà IE., Gigli G., Moroni L., Cortese B., "HYDRHA: Hydrogels of hyaluronic acid. New biomedical approaches in cancer, neurodegenerative diseases, and tissue engineering", Mater Today Bio, 17(August), 2022.
[10] Hu Y., Jia Y., Wang S., Ma Y., Huang G., Ding T., et al., "An ECM-Mimicking, Injectable, Viscoelastic Hydrogel for Treatment of Brain Lesions", Adv Healthc Mater, 12(1), 1–11, 2023.
[11] Güner Yılmaz Ö.Z., Güner F.S., "Hyaluronic Acid-Enriched Pectin-Based Hydrogel Films for Wound Healing", ITU ARI Bull Istanbul Tech Univ, 5(1), 5–22, 2024.
[12] Güner Yılmaz Ö.Z., Yılmaz A., Bozoğlu S., Karatepe N., Batirel S., Şahin A., Güner F.S., "Single-Walled (Magnetic) Carbon Nanotubes in a Pectin Matrix in the Design of an Allantoin Delivery System", ACS Omega, 9(9), 16012–16024, 2024.
[13] Alarcin E., Izbudak B., Erarslan E.Y., Domingo S., Tutar R., Titi K., Kocaaga B., Guner F.S., Bal-Öztürk A., "Optimization of methacrylated gelatin/layered double hydroxides nanocomposite cell-laden hydrogel bioinks with high printability for 3D extrusion bioprinting", J Biomed Mater Res A, 110(10), 1957–1972, 2022.
[14] Liu S., Wei L., Huang J., Luo J., Weng Y., Chen J., "Chitosan/Alginate-Based Hydrogel Loaded With VE-Cadherin/FGF as Scaffolds for Wound Repair in Different Degrees of Skin Burns", J Biomed Mater Res B Appl Biomater, 113(1), 45–57, 2025.
[15] Del Gaudio P., Amante C., Civale R., Bizzarro V., Petrella A., Pepe G., et al., "In situ gelling alginate-pectin blend particles loaded with Ac2-26: A new weapon to improve wound care armamentarium", Carbohydr Polym, 227(August 2019), 115305, 2020.
[16] Kocaaga B., Bagimsiz G., Alev IA., Miavaghi MA., Sirkecioglu A., Batirel S., et al., "Fabrication of MIL-101(Fe)-embedded biopolymeric films and their biomedical applications", Macromol Res, 101(0123456789), 2024.
[17] Alvarez-Lorenzo C., Blanco-Fernandez B., Puga AM., Concheiro A., "Crosslinked ionic polysaccharides for stimuli-sensitive drug delivery", Adv Drug Deliv Rev., 65(9), 1148–71, 2013.
[18] Yang Z., Huang R., Zheng B., Guo W., Li C., He W., et al., "Highly Stretchable, Adhesive, Biocompatible, and Antibacterial Hydrogel Dressings for Wound Healing", Adv Sci, 8(8), 1–12, 2021.
[19] Khan BA., Karim F., Khan MK., Haider F., Khan S., "Synthesis and characterization of polymeric responsive CMC/Pectin hydrogel films loaded with Tamarix aphylla extract as potential wound dressings", Biocell, 45(5), 1273–85, 2021.
[20] Kanikireddy V., Varaprasad K., Jayaramudu T., Karthikeyan C., Sadiku R., "Carboxymethyl cellulose-based materials for infection control and wound healing: A review", Int J Biol Macromol., 164, 963–75, 2020.
[21] Chen YM., Sun L., Yang SA., Shi L., Zheng WJ., Wei Z., et al., "Self-healing and photoluminescent carboxymethyl cellulose-based hydrogels", Eur Polym J, 94(June), 501–10, 2017.
[22] Saha N., Shah R., Gupta P., Mandal BB., Alexandrova R., Sikiric MD., et al., "PVP-CMC hydrogel: An excellent bioinspired and biocompatible scaffold for osseointegration", Mater Sci Eng C, 95(March 2018), 440–9, 2019.
[23] Zhang K yan., Li D., Wang Y., Wang L jun., "Carboxymethyl chitosan/polyvinyl alcohol double network hydrogels prepared by freeze-thawing and calcium chloride cross-linking for efficient dye adsorption", Int J Biol Macromol, 253(August), 2023.
[24] Gupta B., Agarwal R., Sarwar Alam M., "Antimicrobial and release study of drug loaded PVA/PEO/CMC wound dressings", J Mater Sci Mater Med, 2014.
[25] Rahaman MS., Hasnine SMM., Ahmed T., Sultana S., Bhuiyan MAQ., Manir MS., et al., "Radiation crosslinked polyvinyl alcohol/polyvinyl pyrrolidone/acrylic acid hydrogels: swelling, crosslinking and dye adsorption study", Iran Polym J (English Ed), 30(10), 1101–16, 2021.
[26] Sun TY., Liang LJ., Wang Q., Laaksonen A., Wu T., "A molecular dynamics study on pH response of protein adsorbed on peptide-modified polyvinyl alcohol hydrogel", Biomater Sci, 2(3), 419–26, 2014.
[27] Han W., Meng Y., Hu C., Dong G., Qu Y., Deng H., et al., "Mathematical model of Ca2+ concentration, pH, pectin concentration and soluble solids (sucrose) on the gelation of low methoxyl pectin", Food Hydrocoll, 66, 37–48, 2017.
[28] Kim Y., Kim SE., Park KD., Park KM., "Bioadhesives and bioactive hydrogels for wound management", J Control Release, 379(September 2024), 285–302, 2025.
[29] Zhang L., Yin H., Lei X., Lau JNY., Yuan M., Wang X., et al., "A Systematic Review and Meta-Analysis of Clinical Effectiveness and Safety of Hydrogel Dressings in the Management of Skin Wounds", Front Bioeng Biotechnol, 7(November), 1–16, 2019.
[30] Puertas-Bartolomé M., Benito-Garzón L., Fung S., Kohn J., Vázquez-Lasa B., San Román J., "Bioadhesive functional hydrogels: Controlled release of catechol species with antioxidant and antiinflammatory behavior", Mater Sci Eng C, 105(July), 2019.
[31] Ge L., Xu Y., Li X., Yuan L., Tan H., Li D., et al., "Fatty acid-based polyurethane films for wound dressing applications", Macromol Symp, 6(2), 102160, 2021.
[32] Zhao X., Debeli DK., Shan G., "A novel drug loading and release from a thermoresponsive hydrogel formed in situ emulsion polymerization", J Appl Polym Sci, 137(19), 1–10, 2020.

[33] Geever LM., Higginbotham CL., "Temperature-triggered gelation and controlled drug release via NIPAAm/NVP-based hydrogels", J Mater Sci, 46(9), 3233–40, 2011.
[34] Abdelaatti A., Buggy DJ., Wall TP., "Local anaesthetics and chemotherapeutic agents: a systematic review of preclinical evidence of interactions and cancer biology", BJA Open, 10(January), 2024.
[35] Rodoplu S., Celik BE., Kocaaga B., Ozturk C., Batirel S., Turan D., et al., "Dual effect of procaine-loaded pectin hydrogels: pain management and in vitro wound healing", Polym Bull, 2020.
[36] Inguscio CR., Cisterna B., Lacavalla MA., Donati F., Angelini O., Tabaracci G., et al., "Ozone and procaine increase secretion of platelet-derived factors in platelet-rich plasma", Eur J Histochem, 67(4), 241–51, 2023.
[37] Yerlikaya C., "Effect of Different Brewing and Analysis Conditions on Caffeine Content in Tea", Bilecik Seyh Edebali Univ J Sci, 10(2), 363–372, 2023.
[38] Xia Y., Zou S., Xie P., Feng X., "A kind of multi-dot ensemble regression AI detector for lubricating oil additive content based on lambert-beer law", Spectrochim Acta Part A Mol Biomol Spectrosc, 318(February), 1–10, 2024.
[39] Bal-Öztürk A., Torkay G., İdil N., Özkahraman B., Özbaş Z., "Gellan gum/guar gum films incorporated with honey as potential wound dressings", Polym Bull, 81(2), 1211–28, 2024.
[40] Yuk H., Lin S., Ma C., Takaffoli M., Fang NX., Zhao X., "Hydraulic hydrogel actuators and robots optically and sonically camouflaged in water", Nat Commun, 8, 2017.
[41] Subashini M., Devarajan PV., Sonavane GS., Doble M., "Molecular dynamics simulation of drug uptake by polymer", J Mol Model, 17(5), 1141–7, 2011.
[42] Pereira RF., Mendes A., Bártolo PJ., "Novel alginate/aloe vera hydrogel blends as wound dressings for the treatment of several types of wounds", Chem Eng Trans, 32, 1009–14, 2013.
[43] Yao K., Li S., Zheng X., Zhang Q., Liu J., Liang C., et al., "Superwettable calcium ion exchanged carboxymethyl cellulose powder with self-gelation, tissue adhesion and bioabsorption for effective hemorrhage control", Chem Eng J, 481(November 2023), 2024.
[44] Tyagi V., Thakur A., "Carboxymethyl cellulose-polyvinyl alcohol based materials: A review", Mater Today Proc, (xxxx), 2023.
[45] Kumar A., Kumar A., "Development and characterization of tripolymeric and bipolymeric composite films using glyoxal as a potent crosslinker for biomedical application", Mater Sci Eng C [Internet], 73, 333–9, 2017.
[46] Kocaağa B., Öztürk Y., Ceren Kurçin H., Güner-Yılmaz Z., Kurkcuoglu O., Tatlier M., et al., "Developing multifunctional pectin-based hydrogel for wound dressing: In silico, in vitro and in vivo evaluation", Eur Polym J, 216(July), 2024.
[47] Özkaynak MU., Kocaaga B., Dönmez KB., Dağlar S., Türker Y., Karatepe N., et al., "Understanding the role of water in the lyotropic liquid crystalline mesophase of high-performance flexible supercapacitor electrolytes using a rheological approach", J Mol Liq, 394(November 2023), 2024.
[48] Kocaaga B., Inan T., Yasar Nİ., Yalcin CE., Sungur FA., Kurkcuoglu O., et al., "Innovative Use of an Injectable, Self-Healing Drug-Loaded Pectin-Based Hydrogel for Micro- and Supermicro-Vascular Anastomoses", Biomacromolecules, 25(7), 3959–75, 2024.
[49] Alarcin E., Akguner Z.P., Ozturk A.B., Yasayan G., Ilhan-Ayisigi E., Kazan A., Yesil-Celiktaş O., Akcora D.S., Akakin D., Kocaaga B., et al., "Biomimetic 3D bioprinted bilayer GelMA scaffolds for the delivery of BMP-2 and VEGF exogenous growth factors to promote vascularized bone regeneration in a calvarial defect model in vivo", Int. J. Biol. Macromol., 306(Part 2), 141440, 2025.
[50] Roversi T., Piazza L., "Supramolecular assemblies from plant cell polysaccharides: Self-healing and aging behavior", Food Hydrocoll [Internet], 54, 189–95, 2016.
[51] Cao C., Yang N., Zhao Y., Yang D., Hu Y., Yang D., et al., "Biodegradable hydrogel with thermo-response and hemostatic effect for photothermal enhanced anti-infective therapy", Nano Today [Internet], 39, 101165, 2021.
[52] Li S., Wang L., Zhang J., Zhao Z., Yu W., Tan Z., et al., "Combination of natural polyanions and polycations based on interfacial complexation for multi-functionalization of wound dressings", Front Bioeng Biotechnol, 10(September), 1–13, 2022.
[53] Özkahraman B., Torkay G., İdil N., Özbaş Z., Bal-Öztürk A., "Antibacterial, Antioxidant, and Healing Potential of Wound Dressings Utilizing Cranberry Extract in Combination with Methacrylated Polyvinyl Alcohol and Methacrylated Sericin", Regen Eng Transl Med, 577–89, 2024.